

Segregation-induced grain boundary electrical potential in ionic oxide materials: A first principles model

D. Gómez-García (a), Juan J. Meléndez (b), Robert L. González-Romero (a), A. Domínguez-Rodríguez (a)

a Departamento de Física de la Materia Condensada, Universidad de Sevilla, ICSMSE-CSIC, PO Box 1065, 41080 Sevilla, Spain

b Departamento de Física, Universidad de Extremadura, Avenida de Elvas, s/n, 06071 Badajoz, Spain

Referred to by

D. Gómez-García, Juan J. Meléndez, Robert L. González-Romero, A. Domínguez-Rodríguez
Corrigendum to “Segregation-induced grain boundary electrical potential in ionic oxide materials: A first principles model” [Acta Materialia 58 (2010) 6404–6410]

Acta Materialia, Volume 59, Issue 4, February 2011, Page 1848

Abstract

A first principles continuum analytical model for cationic segregation to the grain boundaries in complex ceramic oxides is presented. The model permits one to determine the electric charge density and the segregation-induced electric potential profiles through the grain and can be extrapolated to the range of nanostructured grain sizes. The theoretical predictions are compared with existing data for yttria-stabilized tetragonal zirconia polycrystals. The implications for physical properties (mainly high temperature plasticity and hardening behaviour) are then discussed.

Keywords

Ceramics; Grain boundary defects; Segregation; Analytical methods

1. Introduction

Research on interfaces in complex oxides is today in the forefront of Condensed Matter Physics. The recently reported control of the interface ground state by means of external electric fields has opened up new research lines and potential applications [1], [2] and [3]. In this context, several aspects of the interface physics need to be clarified. Among them, controlling segregation to the grain boundaries is a key issue, particularly when segregation involves a change in the electrical nature of the interface. In practice, this would permit optimized design of new advanced materials. Many structural and functional properties have been found to depend on the physico-chemical nature of boundaries. For instance, mechanical, electrical and optical properties have a strong dependence on the degree of purity of interfaces. For a few systems a full comprehension of segregation and electrical effects already exists. Such is the case for intrinsic oxides, in which double layer segregation theory [4] is able to accurately predict the segregation level to the grain boundaries. In these materials segregation is driven by

the difference in the formation energy of the defect species. A case of more particular interest is that of extrinsic systems, i.e. those in which a certain quantity of metallic cations have been replaced by foreign ions with a different electric charge. Indeed, this case is perhaps the most interesting for technological applications, since mechanical and electrical properties are usually optimized through the addition of substitutional dopants. In this context, and from a fundamental point of view, segregation in doped oxides is a challenging topic in which chemical species are driven to the grain boundaries as a result of various interactions taking place simultaneously.

Although there have been several theoretical approaches to this problem [4], [5] and [6], they are not satisfactory for two main reasons.

1. The grain size is supposed to be large enough that the grain can be treated as an ideal source of defects. The electrical potential is assumed to be unaltered inside the grain. This approximation is not acceptable when one deals with segregation in nanostructured specimens.
2. Even for very large grains, the boundary conditions adopted are incorrect. Indeed, a given value of electrical potential at the grain boundary is commonly assumed. However, such an assumption is incompatible with global electroneutrality, as will be shown later.

No rigorous treatment of this problem has been found in the literature. This paper tries to fill this gap by solving the equations ruling surface segregation in equilibrium with consistent boundary conditions. The results will be extrapolated to the nanoscale range. When applied to a model system (YTZP) the model accounts for many of the experimental findings found in the literature.

2. Theoretical development

2.1. Outline

Let us consider a ceramic material, typically an oxide of a metallic element, in which a certain number of cations have been replaced by either acceptor or donor cations to form a homogeneous alloy. Since the dopant cations have a different electric charge from the host cations, they have an effective electric charge. In addition, electrical neutrality demands a number of oxygen vacancies (which behave as positive charges) to be created in the system, which then becomes non-stoichiometric. A typical example in the scientific literature is the system $Y_2O_3-ZrO_2$ stabilized into a tetragonal phase, usually referred to as YTZP (yttria-stabilized tetragonal zirconia polycrystals) [7]. The charged species present in the system give rise to an electric potential within the grain.

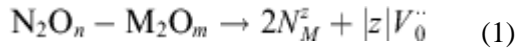
Let us suppose also that the ionic radius of the dopant cations is significantly larger than that of the host cations. In such a case integration of the dopant cations into the host lattice causes some excess elastic energy to be stored around them. This energy may in turn be released through segregation of the dopant species (which are charged) to the free surfaces; for the sake of simplicity, only segregation to the grain boundaries will be considered here. For instance, this effect has been found in the $Y_2O_3-ZrO_2$ system, where the zirconium cation radius is 20% smaller than that of the donor yttrium cation [8].

There are thus two main driving forces for segregation: the elastic misfit effect and interaction of the charged particles with the potential they themselves have created. In equilibrium segregation creates a charged layer and, therefore, a local electric field within the grains. In

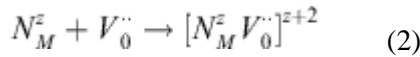
ceramics this field is strongly screened by the mobile charge carriers present in the grains (i.e. the oxygen vacancies). As a consequence, the local electric field extends from the grain boundaries to within the grain interior up to a typical length, the Debye screening length. In other words, there is a non-negligible space charge layer where the electric potential decays. This long scale character of the electric potential gradient is due to the fact that the defects responsible for electric potential screening are oxygen vacancies. A similar mechanism of charge separation may be induced in metals, but, since the mobile charge carriers are the conduction electrons and these are much more effective than the oxygen vacancies in oxides, the local electric field is strongly damped out.

2.2. Formulation of the model

Let us consider a binary metal oxide alloy expressed in general as $N_2O_n - M_2O_m$, with $m > n$. In this system substitutional defects N_M^z will exhibit an effective charge $ze = (n - m)e < 0$, and an appropriate number of oxygen vacancies (charge $+2e$) will appear to compensate this negative electric charge, as expected from the equilibrium equation:



In addition, substitutional defects can be involved in a short-range interaction with oxygen vacancies to form a complex binary defect according to:



Higher order defects can be formed similarly, with progressively smaller volume concentrations. For the sake of simplicity we will restrict the study to this second order approximation (i.e. binary defects).

Let us also consider that the grains are spherical with radius R . In this case all the physical properties involved in this problem are, in equilibrium, functions of the radial coordinate r only. Let n_N^0 , n_V^0 , and n_B^0 denote the nominal bulk volume concentrations of substitutional defects, oxygen vacancies and binary defects in an infinite solid, i.e. a solid where R is sufficiently large that no local electric fields exist. These concentrations depend on temperature according to an Arrhenius function, and they are related to the formation energy of each type of defect according to the mass action law:

$$\frac{(n_B^0)^{z+2}}{n_N^0 n_V^0} (n_N^0 + n_V^0 + n_B^0)^{-z} = K(T) \quad (3)$$

where $K(T)$, which plays the role of an equilibrium constant, is a characteristic constant. In addition, the charge conservation condition leads to:

$$zn_N^0 + 2n_V^0 + (z + 2)n_B^0 = 0 \quad (4)$$

The concentration profiles n_N , n_V , and n_B of the three types of defects in thermodynamic equilibrium are accurately described by the Langmuir–MacLean isotherm [9]:

$$\begin{aligned}
n_N &= n_N^0 \frac{\exp\left(-\frac{\Delta G_N + ze\phi}{k_B T}\right)}{1 + x_N^0 \left[\exp\left(-\frac{\Delta G_N + ze\phi}{k_B T}\right) - 1\right]} \\
n_V &= n_V^0 \frac{\exp\left(-\frac{\Delta G_V + 2e\phi}{k_B T}\right)}{1 + x_V^0 \left[\exp\left(-\frac{\Delta G_V + 2e\phi}{k_B T}\right) - 1\right]} \\
n_B &= n_B^0 \frac{\exp\left(-\frac{\Delta G_B + (z+2)e\phi}{k_B T}\right)}{1 + x_B^0 \left[\exp\left(-\frac{\Delta G_B + (z+2)e\phi}{k_B T}\right) - 1\right]}
\end{aligned} \tag{5}$$

where $\phi = \phi(r)$ is the electric potential inside the grain, x_X^0 (with X standing for substitutional, vacancy or binary defect) the molar fraction of the X species in the grain volume in the absence of segregation, k_B is the Boltzmann constant and T the absolute temperature.

The term ΔGX is the segregation enthalpy for the species X, i.e. the energy released when a defect X segregates to the boundaries; it should be negative because segregation is a favoured process. In a general sense, this term is relevant only for substitutional cations because, while the vacancies and binary defects can move almost freely within the crystalline lattice, the substitutional cations are subjected to the elastic misfit effect due to their different sizes relative to the parent cations [10]. Cahn et al. have reported that the elastic contribution is by far the more intense in most ceramic systems [11]. The segregation enthalpy depends on the distance to the boundaries, having a negligible value at a distance $R-l$ with $l \ll R$. It may be calculated as the sum of two contributions: the first accounting for segregation to a flat (i.e. $R \rightarrow \infty$) layer of thickness δ , and the second for the energy required to bend the flat layer to the actual value of R. Several laws have been proposed for the first contribution [4] and [5]. In the present model a first order approximation will be adopted [5]:

$$\begin{aligned}
\Delta G_{N,1}(r) &= \frac{\Delta G_N^0}{l} (r - R + l) \\
&= \frac{\Delta G_N^0}{\eta} \left(\frac{r}{R} - 1 + \eta\right) \quad \text{for } R - l < r < R
\end{aligned} \tag{6}$$

where $\eta = l/R$ and View the MathML source is the maximum value of the segregation enthalpy, which depends on the elastic parameters and the ionic radii of the host and dopant cations in the system under study.

The second contribution, $\Delta GN,2(r)$, may be computed from elastic theory [10] as follows. The pressure due to the curved boundaries is proportional to the dilation E of a small layer of thickness l and surface area $4\pi R^2$ when strained to fully cover a spherical surface of radius R, i.e.

$$E = \frac{\Delta V}{V} = \frac{4\pi R^2 l - \frac{4}{3}\pi R^3 [1 - (1 - \eta)^3]}{\frac{4}{3}\pi R^3 [1 - (1 - \eta)^3]} = \frac{\eta}{3} \frac{1 - \frac{\eta}{3}}{1 - \eta + \frac{\eta^2}{3}} \tag{7}$$

The pressure at the curved boundary is just the product of the dilation and the bulk modulus

$$\left(B = \frac{2\mu(1+\nu)}{3(1-2\nu)}\right)$$

The second contribution $\Delta G_{N,2}(r)$ is then

$$\Delta G_{N,2} = \frac{2\mu(1+\nu)\Omega}{9(1-2\nu)} \frac{\eta(1-\frac{\eta}{3})}{1-\eta+\frac{\eta^2}{3}} \quad \text{for } R-l < r < R \quad (8)$$

with μ being the shear modulus, Ω the cation volume, and ν the Poisson ratio of the solute.

Given the segregation enthalpies, and according to Eq. (4), the local concentration of each species may be calculated from the electric potential $\phi(r)$, which in turn is given by the Poisson equation for the grain:

$$\nabla^2 \phi = \frac{\rho}{\epsilon} = \frac{e}{(\epsilon[z n_N + 2n_V + (z+2)n_B])} \quad (9)$$

where ρ is the local effective electric charge within the grain and ϵ is the dielectric constant of the grain. The right-hand side of Eq. (9) is a (non-linear) function of the electric potential.

To solve this equation, one must set the proper boundary conditions. For a general geometry these arise from the electroneutrality of the grain as a whole, which leads to:

$$\int_V \nabla^2 \phi dV = 0 \quad (10)$$

i.e. applying divergence's theorem:

$$\int_{\text{Grain boundary}} \nabla \phi \cdot \mathbf{n} dS = 0 \quad (11)$$

where \mathbf{n} is an outward unit vector normal to the surface of the grain at each point and the surface integral extends to the whole grain boundary. Note that these conditions do not fix the potential value at any point in the grain, because Poisson's Eq. (9) is not invariant under the addition of an arbitrary constant to the electric potential.

In the case that we are considering here (i.e. a spherical grain of radius R) symmetry conditions allow one to conclude that $\phi(r)$ is an even function, so that an extremum is expected at $r = 0$:

$$\left(\frac{d\phi}{dr}\right)_{r=0} = 0 \quad (12)$$

On the other hand, Eq. (11) reduces here to a single condition, namely:

$$\left(\frac{d\phi}{dr}\right)_{r=R} = 0 \quad (13)$$

This choice of boundary conditions is not particularly critical for very large grain sizes, but is extremely important when one extrapolates to the nanoscale. In this case the mathematical results will depend strongly on the choice of boundary conditions. To the best of the authors' knowledge this subtle detail had never been taken into consideration before.

3. Results and discussion

3.1. The $K = 0$ limit

A limiting case which deserves particular attention is that in which the number of binary defects is assumed to be negligible, i.e. $K = 0$ in Eq. (3). This may occur when the solution is very dilute or the temperature is very high. In the $K = 0$ limit the molar fractions View the MathML source appearing in Eq. (5) are also negligible, so that the concentrations of metallic cations and oxygen vacancies are simply given by:

$$n_N(r) = n_N^0 \exp\left(-\frac{\Delta G_N + ze\phi}{k_B T}\right) \quad (14)$$

$$n_V(r) = n_V^0 \exp\left(-\frac{2e\phi}{k_B T}\right) \quad (15)$$

where it has been assumed that they can move freely within the grains. Substitution of Eqs. (14) and (15) into Eq. (9) yields:

$$\frac{1}{r^2} \frac{d}{dr} \left[r^2 \frac{d\phi}{dr} \right] = \frac{e}{\epsilon} \left[zn_N^0 \exp\left(-\frac{\Delta G_N + ze\phi}{k_B T}\right) + 2n_V^0 \exp\left(-\frac{2e\phi}{k_B T}\right) \right] \quad (16)$$

Introducing the reduced dimensionless variables

$$\begin{aligned} y &= \frac{r}{R} \\ \tilde{\phi} &= \frac{e\phi}{k_B T} \\ \Delta \tilde{G}_N &= \frac{\Delta G_N}{k_B T} \end{aligned} \quad (17)$$

and taking into account the condition (4) for electrical neutrality (with View the MathML source), Eq. (16) may be rewritten as:

$$\frac{1}{y^2} \frac{d}{dy} \left(y^2 \frac{d\tilde{\phi}}{dy} \right) = z\delta^2 \left[k \exp(-z\tilde{\phi}) - \exp(-2\tilde{\phi}) \right] \quad (18)$$

with $\kappa = \exp(-\Delta \tilde{G}_N)$ and $\delta = R/\lambda$, where

$$\lambda = \left(\frac{\epsilon k_B T}{n_N^0 e^2} \right)^{\frac{1}{2}} \quad (19)$$

is Debye's screening length.

Eq. (18) was solved for a model system, as will be shown below. However, one can find analytical solutions of Eq. (18) by making different assumptions within the $K = 0$ limit. For instance, there is a trivial solution for $k = 1$, whose physical meaning is clear: unless there is a

non-electrical driving force imposing separation on the charges, electroneutrality is verified locally and there is no electric field within the grain.

Let us now take $k \neq 1$ and suppose that the temperature is high enough that the reduced potential satisfies View the MathML source. Since the higher the temperature the greater the thermal disorder, the tendency to segregate to the free surfaces must decrease and the exponentials on the right-hand side of Eq. (18) may be expanded in Taylor series. To first order this gives:

$$\frac{1}{y^2} \frac{d}{dy} \left(y^2 \frac{d\tilde{\phi}}{dy} \right) \approx z\delta^2 \left[(k-1) + (2-kz)\tilde{\phi} \right] \quad (20)$$

which is the linearized form of Eq. (18). The solution of Eq. (20) is detailed in the Appendix.

3.2. High temperature grain size dependence of the grain boundary potential

Many physical properties, for instance electrical or mechanical, are found to depend only on the grain boundary potential difference View the MathML source $\tilde{\phi}(1) - \tilde{\phi}(0)$ so there is no need for the detailed solution of Eq. (9). Instead, it is interesting to see how this quantity depends on grain size. Note that the leading parameters of this problem are η and δ . The former is the thickness of the segregation layer in reduced units and the latter scales the length at which the electric effects die out inside the grain. Note also that $\delta\eta = 1/\lambda$, which is a dimensionless parameter depending only weakly on temperature.

Two limiting cases may then be distinguished.

(a)

Large grain limit, $\delta \gg 1$ and hence $\eta \ll 1$. In this case the electric field is strongly damped out, so the potential only varies appreciably in the neighbourhood of the grain boundary $\tilde{\phi}(1)$ (i.e. $\tilde{\phi}(y) \cong 0$ for $y \leq 1 - \eta$). As a first approximation, an approximate solution of Eq. (18) can be obtained by setting $\tilde{\phi}(y) = \tilde{\phi}(1)$ on the right-hand side and averaging. This calculation yields

$$\frac{1}{y^2} \frac{d}{dy} \left(y^2 \frac{d\tilde{\phi}}{dy} \right) = \frac{\delta^2}{2} \left\{ zk_0 e^{-z\tilde{\phi}(1)} - [z + (2+z)\alpha] e^{-2\tilde{\phi}(1)} + (2+z)\alpha e^{-(2+z)\tilde{\phi}(1)} \right\} \quad (21)$$

where $k_0 = k(1) = e^{\Delta\tilde{G}_{N0}}$ and $\alpha = \frac{n_B^0}{n_N^0}$. With the boundary condition (12), and taking $\tilde{\phi}(0) = 0$, a transcendental equation for $\tilde{\phi}(1)$ is obtained:

$$\frac{\tilde{\phi}(1)}{zk_0 \exp[-z\tilde{\phi}(1)] - [z + (2+z)\alpha] \exp[-2\tilde{\phi}(1)] + (2+z)\alpha \exp[-(2+z)\tilde{\phi}(1)]} = -\frac{(\delta\eta)^2}{12} \frac{\eta - 3}{\eta - 1} \quad (22)$$

which implies that the electric potential is only slightly dependent on the grain size. This is the limiting case of a planar-like grain boundary.

(b)

Small grain limit, $\delta \leq 1$. Let us now assume that the solution of Eq. (18) is analytical in δ , so that it admits a power expansion in δ :

$$\tilde{\phi}(y) = \tilde{\phi}_0(y) + \tilde{\phi}_1(y)\delta + \tilde{\phi}_2(y)\delta^2 + \dots + \tilde{\phi}_n(y)\delta^n \quad (23)$$

Substituting Eq. (23) into Eq. (18) and regrouping the terms one has the following hierarchy of equations:

$$\nabla^2 \tilde{\phi}_0 = 0 \quad (24)$$

$$\nabla^2 \tilde{\phi}_1 = 0 \quad (25)$$

$$\nabla^2 \tilde{\phi}_2 = z(k(y) - 1) \quad (26)$$

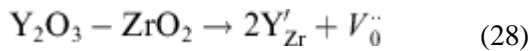
and so on. Eqs. (24) and (25) are easy to solve if it is admitted that $k(y) \cong k_0$, a constant value, for $1 - \eta \leq y \leq 1$ and zero elsewhere. A lengthy calculation yields the following expression for the potential difference:

$$\tilde{\phi}(1) - \tilde{\phi}(0) \cong \frac{z}{6} \left(\frac{l}{\lambda} \right)^2 (k_0 - 1) \quad (27)$$

The potential difference decreases with δ down to a minimum value given by Eq. (27). This value is of the order of a few millivolts.

3.3. General solutions for a model system

The above theoretical development will be checked by applying it to a model system, YTZP, which is by far one of the most studied groups of ceramic alloys due to their excellent mechanical and electrical properties at moderate temperatures [12]. These properties are the result of the presence of substitutional yttrium atoms in zirconium positions, having an effective electric charge $z = -1$, together with oxygen vacancies to maintain overall electroneutrality. This mechanism can be expressed in Kröger–Vink notation as follows:



The existence of oxygen vacancies accounts for a high ionic conductivity at temperatures as low as 800 °C, whereas the numerous substitutional yttrium defects are responsible for high temperature plasticity, since they determine the value of the cationic diffusion coefficients. Regarding the mechanical properties, the role of the yttrium defects is not restricted to only determining the diffusion coefficients, but also affects these properties through the electric potential generated at the grain boundaries [13], [14], [15], [16], [17] and [18]. Binary defects must also be taken into account [12]. For this particular case, Eq. (3) reduces to:

$$\frac{n_B^0}{n_N^0 n_V^0} (n_N^0 + n_V^0 + n_B^0) = K(T) \quad (29)$$

Eq. (9) was thus solved for YTZP using a set of input parameters (Debye screening length, segregation enthalpies and characteristic constant) available in the literature (Table 1). These data were obtained at creep temperatures, which is coherent with the hypotheses made above.

Fig. 1 displays the potential profile for different grain sizes ($d = 2R$) at a reference temperature $T = 1473$ K. The potential is negative, as expected, because the induced electric field along the grain impedes further segregation to the boundaries. For small grains the potential profile is almost flat (i.e. the electric field is negligible within the grain) because the local concentrations of each type of defect do not vary much within the grain volume. As the grain size increases the electric potential at the centre of the grain approaches zero, whereas the potential profiles undergo a sharp decrease as one gets close to the grain boundary. The region where this decrease appears corresponds to the region where the screening charges (here oxygen vacancies) must mainly be located. Note also that the width of this screening region decreases with increasing grain size. Finally, comparison of the grain boundary potential View the MathML source with experimental data in the literature [6], [12], [19], [20] and [21] shows very good agreement with our theoretical values (0.1–0.2 V in the same temperature range).

Fig. 2 displays the enhancement profile factors (i.e. the ratios $n_X(y)/$ View the MathML source) for yttrium cations, oxygen vacancies and binary defects. All these factors increase with the reduced grain size y , which indicates that segregation tends to agglomerate all the defects near the grain boundaries. It is particularly interesting that there is a real enhancement of the number of oxygen vacancies when moving to the grain boundaries, to the detriment of the bulk concentration. This observation seems to go against some statements in the literature which argue for a depletion of the concentration of oxygen vacancies at the grain boundaries relative to the bulk concentration. However, there is no real contradiction, because our results indicate that it is the ratio between the oxygen vacancy and yttrium cation concentrations which decreases when moving towards the grain boundary. Thus, there is an effective, but not real, depletion of positive charges. The oxygen vacancies, whose concentration relative to that for the yttrium cations is significantly greater at some distance from the grain boundary (between around $y = 0.85$ and $y = 0.97$ in Fig. 2), screen the electric field created by the negative charges (whose concentration is higher at $y > 0.97$, approximately), so that it is roughly zero within the grain interior, in good agreement with the results shown in Fig. 1. In addition, although there are no data for YTZP, these profiles are also in very good agreement with those reported in the literature for yttrium segregation to the boundaries in Y_2O_3 – TiO_2 alloys, a system which is comparable with yttria–zirconia in terms of elastic misfit parameters and segregation energies [22].

Fig. 3 shows the grain size dependence of the boundary electric potential (relative to the value at the centre of the grain). Several data series are included in Fig. 3. The first two were calculated with the $K = 0$ approximation (Eq. (18)), either assuming that segregation takes place at a flat boundary (i.e. $\Delta G_{N,2} = 0$) or taking the curvature of the grain into account. From Fig. 3 it is straightforward to conclude that the curvature of the grain does not have any effect on the electric potential. Therefore, regardless of the grain size, it suffices to consider segregation to a flat boundary; subsequent calculations were performed neglecting the term $\Delta G_{N,2}$ in the segregation enthalpy. The third series of data was calculated explicitly considering the segregation of binary defects at a flat boundary. As observed, the introduction of binary defects has a significant effect on the values of the grain boundary potential (lowering it by around 10%). This means that binary defects must always be taken into account for any accurate measurement of grain boundary potential, even at temperatures as high as 1200 °C. It is noteworthy that this fact had been ignored until now when analysing electrical and mechanical properties.

The electric potential does not depend on the grain size for large grain size values (typically values >200 nm, stage III in Fig. 3); the near independence of $\bar{\phi}(1)$ on the grain size in stage III is fully consistent with the fact that one is approaching a semi-infinite system with a flat boundary. For smaller values the potential decreases (in absolute value) sharply to reach a plateau (stage II in Fig. 3) at approximately 180 nm, as was observed experimentally by Theuissen et al. [23]. Thereafter $\bar{\phi}(1)$ remains almost constant until a value of approximately 40 nm, from where the electric potential decreases smoothly to zero (stage I in Fig. 3). Hence, for very small grains the electric potential is zero inside the grain, since the concentration of defect species is practically unaltered by segregation.

This behaviour accounts for the peculiar mechanical properties of Y₂O₃–ZrO₂ alloys. Since a polycrystal is composed of a large number of grains of different sizes, it may be assumed that neighbouring grains have different sizes. When this is the case in an insulator, a potential difference should arise across the borders between adjacent grains, with the region behaving as a capacitor, as reported elsewhere [24]. Relative displacement of grain interfaces will require overcoming an energy barrier – the energy stored in the capacitor. Therefore, a frictional force against grain sliding is induced at the macroscopic scale. This frictional force is commonly identified as the “threshold stress” for the onset of grain boundary sliding-driven plasticity. Experimental evidence of the existence of a threshold stress has repeatedly been described in the literature [24]. The results shown in Fig. 3 permit one to go one step further in understanding that threshold stress on the nanoscale. When the average grain size is within stage II only grains located in the lower tail of the distribution would potentially be affected by the “capacitor” effect described above. Additionally, the smaller the mean grain size, the fewer the grains potentially contributing to the threshold stress. A consequence of this is the fact that the threshold stress decreases monotonically with the mean grain size on the nanoscale.

Despite the tendency exhibited by the threshold stress, the existence of a non-null electric potential at the boundaries does affect cation diffusion within the grains and, hence, the matter transport mechanisms accommodating high temperature plasticity. The main effect is the inhibition of matter transport kinetics, producing a remarkable hardening behaviour at the nanoscale ($40 \text{ nm} < d < 100 \text{ nm}$); the two effects (the threshold stress becoming almost negligible and the resulting increased hardening) are simultaneous and compatible [14] and [24].

Finally, one notable prediction stands out: when the main grain size is well below 40 nm (stage I in Fig. 3) the electric potential approaches zero quite sharply. Assuming a narrow grain size distribution, electric potential-induced hardening and threshold stress would be practically zero. In consequence, the plasticity would be strongly enhanced. This prediction may open a new avenue in the search for optimized superplasticity in ceramic oxides.

Acknowledgements

The authors wish to acknowledge the financial support awarded by the Spanish Research authorities through the Projects MAT2009-14351-C02-01 and MAT2009-14351-C02-02. D.G.G. would like to acknowledge the encouraging scientific atmosphere found in the Tokyo Research Institute during his stays at that institution, hosted by Prof. F. Wakai and sponsored by the Japan Society for the Promotion of Science.

Appendix A

Let us consider the linearized form of Eq. (9):

$$\frac{1}{y^2} \frac{d}{dy} \left(y^2 \frac{d\tilde{\phi}}{dy} \right) = z\delta^2 \left[(k-1) + (2-kz)\tilde{\phi} \right] \quad (\text{AI.1})$$

For $0 \leq y \leq 1 - \eta$ one has the value $k = 1$, so that Eq. (AI.1) reduces to

$$\frac{1}{y^2} \frac{d}{dy} \left(y^2 \frac{d\tilde{\phi}_i}{dy} \right) = z\delta^2 (2-z)\tilde{\phi}_i \quad (\text{AI.2})$$

whose solution, given the condition $\left(\frac{d\tilde{\phi}_i}{dy} \right)_{y=0} = 0$, is

$$\tilde{\phi}_i(y) = C_1 \frac{\cosh \delta_i y}{y} \quad (\text{AI.3})$$

with $\delta_i = \delta[z(2-z)]^{1/2}$. For $1 - \eta \leq y \leq 1$ one has:

$$\frac{1}{y^2} \frac{d}{dy} \left(y^2 \frac{d\tilde{\phi}_e}{dy} \right) = z\delta^2 \left[(k-1) + (2-kz)\tilde{\phi}_e \right] \quad (\text{AI.4})$$

whose solution is:

$$\tilde{\phi}_e(y) = C_2 \frac{\sinh \delta_e y}{y} + C_3 \frac{\cosh \delta_e y}{y} + \frac{k-1}{kz-2} \quad (\text{AI.5})$$

with $\delta_e = \delta[z(2-kz)]^{1/2}$. Functions (AI.3) and (AI.5) and their derivatives must be continuous at $y = 1 - \eta$. In addition, they must be consistent with the electro-neutrality of the whole grain:

$$\int_{\text{Grain}} \rho(r) dV = \epsilon_0 \int_{\text{Grain}} \nabla^2 \phi(r) dV = 0 \quad (\text{AI.6})$$

which, after some algebraic manipulations, may be written as:

$$\int_0^{1-\eta} d \left(y^2 \frac{d\tilde{\phi}_i}{dy} \right) + \int_{1-\eta}^1 d \left(y^2 \frac{d\tilde{\phi}_e}{dy} \right) = 0 \quad (\text{AI.7})$$

Eq. (AI.7) with the boundary conditions leads then to the following system for constants C_1 , C_2 and C_3 :

$$\begin{aligned}
C_1 \cosh \delta_i(1 - \eta) - C_2 \sinh \delta_e(1 - \eta) - C_3 \cosh \delta_e(1 - \eta) &= \frac{k-1}{kz-2}(1 - \eta) \\
C_1 \delta_i \sinh \delta_i(1 - \eta) - C_2 \delta_e \cosh \delta_e(1 - \eta) - C_3 \delta_e \sinh \delta_e(1 - \eta) &= \frac{k-1}{kz-2} \\
C_2(\delta_e \cosh \delta_e - \sinh \delta_e) + C_3(\delta_e \sinh \delta_e - \cosh \delta_e) &= 0
\end{aligned} \tag{AI.8}$$

References

- [1] A.D. Caviglia, S. Cariglio, N. Reyren, D. Jaccard, T. Schneider, M. Gabay et al.
Lett Nat, 456 (2008), p. 624
- [2] K.P. McKenna, A.L. Shluger
Nat Mater, 7 (2008), p. 859
- [3] D.G. Schlom, C.H. Ahn
Nature, 456 (2008), p. 582
- [4] A.P. Sutton, R.W. Balluffi
Interfaces in crystalline materials
Oxford University Press, New York (1995)
- [5] M.F. Yan, R.M. Cannon, H.K. Bowen
J Appl Phys, 54 (1983), p. 764
- [6] X. Guo, J. Maier
J Electrochem Soc, 148 (2001), p. E121
- [7] I.W. Chen, L.A. Xue
J Am Ceram Soc, 73 (1990), p. 2585
- [8] T.G. Nieh, J. Wadsworth, O.D. Sherby
Superplasticity in metals and ceramics
Cambridge University Press, Cambridge, UK (1997)
- [9] P. Flewit, R. Wild
Grain boundaries: their microstructure and chemistry
John Wiley & Sons, Chichester, UK (2001)
- [10] L.D. Landau, E.M. Lifshitz
Theory of elasticity
Pergamon Press, London (1986)
- [11] J. Cahn
Physical metallurgy
Elsevier Science, Amsterdam (1983)

- [12] T. Oyama, M. Yoshida, H. Matsubara
Phys Rev B, 71 (2005), p. 224105
- [13] S. Hwang, I. Cheng
J Am Ceram Soc, 73 (1990), p. 3269
- [14] D. Gómez-García, C. Lorenzo-Martín, A. Muñoz-Bernabé, A. Domínguez-Rodríguez
Phys Rev B, 67 (2003), p. 144101
- [15] C. Lorenzo-Martín, D. Gómez-García, A. Gallardo-López, A. Domínguez-Rodríguez, R. Chaim
Scr Mater, 50 (2004), p. 1151
- [16] A. Domínguez-Rodríguez, D. Gómez-García, C. Lorenzo-Martín, A. Muñoz-Bernabé
J Eur Ceram Soc, 23 (2003), p. 2969
- [17] C.H. Hsueh, P.F. Becher
Phys Rev B, 71 (2005), p. 014115
- [18] K. Nakatani, H. Nagayama, H. Yoshida, T. Yamamoto, T. Sakuma
Scr Mater, 49 (2003), p. 791
- [19] F.R. Chien, A.H. Heuer
Philos Mag A, 73 (1996), p. 681
- [20] X. Guo, R. Waser
Solid State Ionics, 173 (2004), p. 63
- [21] X. Guo, Z. Zhang
Acta Mater, 51 (2003), p. 2539
- [22] Q. Wang, G. Lian, E.C. Dickey
Acta Mater, 52 (2004), p. 809
- [23] G.S.A.M. Theuissen, A.J.A. Winnubst, A.J. Burgraaf
J Mater Sci, 27 (1992), p. 5057
- [24] D. Gómez-García, C. Lorenzo-Martín, A. Muñoz-Bernabé, A. Domínguez-Rodríguez
Philos Mag, 83 (2003), p. 93

Figure captions

Figure 1. Potential profile vs. r/R evaluated from Eq. (9) at 1473 K.

Figure 2. Ratio n_X/n_X^0 vs. r/R for the different defects considered in the model

Figure 3. Grain boundary potential vs. grain size calculated at 1473 K. The inset shows the detail of stages I and II.

Table 1

Table 1. Experimental values reported in the literature for the input parameters of the model.

Experimental quantities	Reported values
λ	5–6 nm [6], [11], [12], [13], [14], [15], [18] and [19]
ΔG_N	0.5 eV [5] and [11]
ΔG_V	0 [11]
ΔG_B	0 [11]
K	$\exp(0.41/k_B T)$ [18]
δ	3 nm [5]

Figure 1

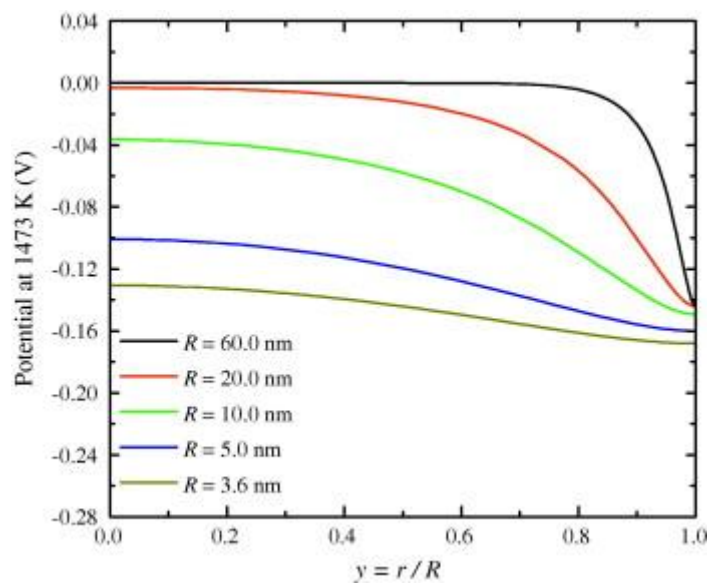


Figure 2

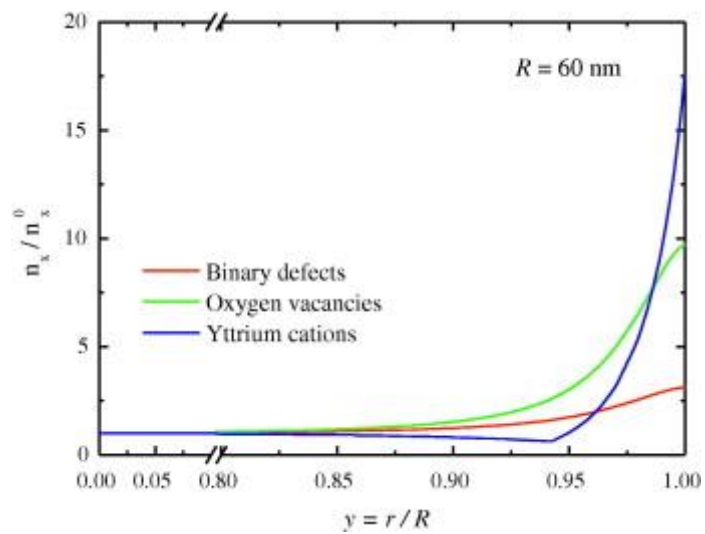


Figure 3

